

Biochemical characterization of Bombyx mori
 α -N-acetylgalactosaminidase belonging to the
glycoside hydrolase family 31

メタデータ	言語: eng 出版者: 公開日: 2021-04-05 キーワード (Ja): キーワード (En): 作成者: Ikegaya, Marina, Miyazaki, Takatsugu, Park, Enoch Y. メールアドレス: 所属:
URL	http://hdl.handle.net/10297/00028133

1 **Biochemical characterization of *Bombyx mori* α -N-acetylgalactosaminidase belonging to**
2 **the glycoside hydrolase family 31**

3

4 Marina Ikegaya¹, Takatsugu Miyazaki^{1,2*}, and Enoch Y. Park^{1,2}

5

6 ¹ Department of Agriculture, Graduate School of Integrated Science and Technology, Shizuoka
7 University, 836 Ohya, Suruga-ku, Shizuoka, 422-8529, Japan.

8

9 ² Green Chemistry Research Division, Research Institute of Green Science and Technology,
10 Shizuoka University, 836 Ohya, Suruga-ku, Shizuoka, 422-8529, Japan.

11

12 ***Correspondence:** Takatsugu Miyazaki, Green Chemistry Research Division, Research
13 Institute of Green Science and Technology, Shizuoka University, 836 Ohya, Suruga-ku,
14 Shizuoka, 422-8529, Japan; Tel: +81-54-238-4886; E-mail:
15 miyazaki.takatsugu@shizuoka.ac.jp

16

17 **Running Title:** *Bombyx mori* GH31 α -N-acetylgalactosaminidase

18

19 **Acknowledgments**

20 We thank Dr. Jun Takeuchi for helping in the ITC experiment. This work was supported in part
21 by the Japan Society for the Promotion of Science (KAKENHI grant No. 19K15748 to TM).

22 We also thank Enago (www.enago.jp) for the English language review. The authors have no
23 conflicts of interest to declare.

24 **Abstract**

25 Horizontal gene transfer is an important evolutionary mechanism not only for bacteria but
26 also for eukaryotes. In the domestic silkworm *Bombyx mori*, a model species of lepidopteran
27 insects, some enzymes are known to have been acquired by horizontal transfer; however, the
28 enzymatic features of protein BmNag31, belonging to glycoside hydrolase family 31 (GH31)
29 and whose gene was predicted to be transferred from *Enterococcus* sp., are unknown. In this
30 study, we reveal that the transcription of *BmNag31* increases significantly during the prepupal
31 to pupal stage, and decreases in the adult stage. The full-length BmNag31 and its truncated
32 mutants were heterologously expressed in *Escherichia coli* and characterized. Its catalytic
33 domain exhibits α -N-acetylgalactosaminidase activity and the carbohydrate-binding module
34 family 32 domain shows binding activity toward N-acetylgalactosamine, similar to the
35 *Enterococcus faecalis* homolog, EfNag31A. Gel filtration chromatography and blue native
36 polyacrylamide gel electrophoresis analyses indicate that BmNag31 forms a hexamer whereas
37 EfNag31A is monomeric. These results provide insights into the function of lepidopteran GH31
38 α -N-acetylgalactosaminidase.

39

40

41 **Keywords:** α -N-acetylgalactosaminidase, *Bombyx mori*, glycoside hydrolase family 31,
42 horizontal gene transfer, hexamer

43

44 **Abbreviations:** α GalNAcase, α -N-acetylgalactosaminidase; CBM, carbohydrate-binding
45 module; FN3, fibronectin type 3; GalNAc, N-acetylgalactosamine; GH, glycoside hydrolase;
46 GH31, glycoside hydrolase family 31; GlcNAc, N-acetylglucosamine; HGT, horizontal gene
47 transfer; ITC, isothermal titration calorimetry; MBP, maltose-binding protein

48

49 **Introduction**

50 Horizontal gene transfer (HGT) is a common means of obtaining new genes in bacteria.
51 There is also a considerable number of genes in animals, including insects, that have been
52 derived from HGT. In insects, some horizontally transferred genes encode functional proteins
53 that may have played an important role in their evolution (Sieber et al., 2017).

54 *Bombyx mori* is a model lepidopteran species whose genome has been repeatedly
55 sequenced by several projects (Goldsmith et al., 2005; Kawamoto et al., 2019; Lu et al., 2020).
56 The resulting genomic information has accelerated the pace of research in Lepidoptera, for
57 example, bioinformatic analysis has revealed that *B. mori* and other lepidopteran species
58 possess several genes obtained by HGT (Li et al., 2011; Sun et al., 2013; Zhu et al., 2011). Some
59 of these genes encode functional enzymes, e.g., chitinase BmChi-h (Daimon et al., 2003; Liu
60 et al., 2017), β -fructofuranosidase BmSUC1 (Daimon et al., 2008; Miyazaki et al., 2020), and
61 4,5-DOPA dioxygenase (Wang et al., 2019). BmChi-h and BmSUC1 are glycoside hydrolases
62 (GHs) belonging to the glycoside hydrolase families GH18 and GH32, respectively, based on
63 their amino acid sequences according to the CAZy database (<http://www.cazy.org>) (Lombard
64 et al., 2014). BmChi-h is a chitinase expressed in the epidermis and midgut during the molting
65 process, a time when the chitin cuticle undergoes degradation. BmSUC1 is a β -
66 fructofuranosidase that is expressed in the midgut and silk glands to digest sucrose. In *B. mori*,
67 *BmNag31* encodes a glycoside hydrolase belonging to glycoside hydrolase family 31 (GH31).
68 Phylogenetic analysis indicates that the ancestral *BmNag31* was acquired *via* HGT from
69 *Enterococcus* sp., most likely the bacterium *Enterococcus faecalis* (Wheeler et al., 2013). *E.*
70 *faecalis*, one of the major gut bacteria in the human intestine, is also found in the midgut of
71 silkworms (Chen et al., 2018; Qin et al., 2010). In the silkworm, *BmNag31* is located on the
72 28th chromosome as a single-copy gene with no introns, thus supporting the HGT-mediated
73 acquisition hypothesis (Li et al., 2011; Wheeler et al., 2013).

74 GH31 is a large family comprising diverse enzymes with various substrate specificities and
75 reaction mechanisms. It includes GHs such as α -glucosidase (Kashiwabara et al., 2000), α -
76 xylosidase (Lovering et al., 2005), and α -galactosidase (Miyazaki and Park, 2020); and it also
77 includes transglycosidases (Aga et al., 2002) and α -glucan lyases (Rozeboom et al., 2013).
78 Aside from BmNag31, most of the other GH31 proteins encoded on the *B. mori* genome share

79 homology with metabolic enzymes in animals, such as endoplasmic reticulum α -glucosidase II
80 and acid α -glucosidase, which are involved in *N*-glycan processing (Watanabe et al., 2013;
81 D'Alessio and M. Dahms, 2015) and lysosomal degradation of glycogen (Roig-Zamboni et al.,
82 2017), respectively. However, because of the divergence among the members of GH31, it is
83 difficult to predict the enzymatic activities and substrate specificities of other uncharacterized
84 GH31 enzymes that share low sequence homologies with characterized enzymes.

85 A recent report indicates that the GH31 proteins, BpGH31 and BcGH31, from the human
86 gut bacteria *Phocaeicola plebeius* (formerly *Bacteroides plebeius*) and *Bacteroides caccae*,
87 respectively, exhibit α -*N*-acetylgalactosaminidase (α GalNAcase) activity, removing the *O*-
88 linked α -*N*-acetylgalactosamine (GalNAc) residue from a glycopeptide but not the blood type
89 A antigen (Rahfeld et al., 2019). Moreover, we recently determined the crystal structure of
90 GH31 α GalNAcase (EfNag31A) from *E. faecalis* (Miyazaki and Park, 2020). The sequence of
91 its xenolog, BmNag31, is 39.9%–52.5% identical to them. However, its physiological role and
92 enzymatic activity remain unclear. To elucidate the function of BmNag31, we cloned the
93 *BmNag31* gene, investigated the properties of the enzyme, and compared them with the
94 properties of EfNag31A.

95

96

97 **Results**

98

99 **Primary structure of Nag31 and comparison with orthologs in other lepidopteran species**

100 BmNag31 consists of three domains: the GH31 catalytic domain, FN3 domain, and
101 CBM32 domain. A bacterial homolog, EfNag31A, shares 52.5% sequence identity with
102 BmNag31, and has a similar domain organization, except that the dockerin, cohesin, and
103 repeating FIVAR domains, and the transmembrane regions follow the CBM32 domain at the C
104 terminus. It should be noted that EfNag31A possesses an N-terminal secretion signal peptide,
105 whereas BmNag31 has no signal peptide based on SignalP prediction server (Fig. 1). In addition,
106 DeepLoc-1.0 and SilkDB predicted that the BmNag31 is localized in cytoplasm (Fig. S1). These
107 features imply that BmNag31 is not a secretory protein, thus it differs from EfNag31A, which
108 may be secreted and works on the cell surface of *E. faecalis* (Miyazaki and Park, 2020).

109 Our BLAST searches against the InsectBase and NCBI protein databases yielded 19
110 sequences which we aligned with the EfNag31A sequence. All lepidopteran BmNag31
111 homologs (Nag31s), as well as BmNag31, were predicted to have no signal peptide at their N
112 termini (Fig. S2). The catalytic residues (predicted nucleophile Asp407 and general acid/base
113 Asp460 in BmNag31) and residues involved in GalNAc recognition were mostly conserved in
114 all available lepidopteran Nag31 proteins, except for the Nag31 protein from *Manduca sexta*
115 (Fig. S2). All available lepidopteran Nag31s have no additional C-terminal domain following
116 the CBM32 domain. By comparing the gene sequences between *B. mori* and *Danaus plexippus*,
117 Wheeler et al. estimated that the HGT between a bacterium and their common ancestor
118 lepidopteran insect occurred at least 65 million years ago (Wheeler et al., 2013). Many
119 lepidopteran genome analyses showed that Nag31 genes are widely distributed in many
120 lepidopteran insects. The estimated divergence time of the most phylogenetically distant species,
121 *Plutella* and *Bombyx*, is about the middle of the Cretaceous (Kawahara et al., 2019), suggesting
122 that HGT occurred 120 million years ago or earlier.

123

124 **Expression analysis of BmNag31**

125 The transcription levels of *BmNag31* in the Malpighian tubule, testis, and ovary were 3–5
126 times higher than that in the fat body of day-3 fifth-instar larvae (Fig. 2A). The transcription
127 levels of *BmNag31* remained stable in the whole bodies of the first- to fifth-instar larvae. Then,
128 the expression level increased remarkably (up to 60 times higher than that of the day-3 fifth-
129 instar larva) from the prepupal stage until day-4 pupa. The expression level then significantly
130 decreased at the adult stage (Fig. 2B). Therefore, the transcription levels of BmNag31 were
131 suggested to depend on the developmental stages rather than the organs. Because *BmNag31*
132 gene is predicted to have been derived from the midgut symbiont *Enterococcus* sp., the
133 expression levels of *BmNag31* in the midgut during different stages were also examined. In the
134 midgut, the expression level of *BmNag31* also increased during the pupal stage (up to 11 times
135 higher than that of the day-3 fifth-instar larva), but this change was minor compared to that of
136 the whole body (Fig. 2C).

137

138 **Oligomerization of BmNag31**

139 The recombinant proteins, maltose-binding protein-fused BmNag31 (MBP-BmNag31) and
140 the GH31 catalytic domain containing a fibronectin type 3 (FN3) domain (named BmGH31)
141 were successfully expressed in *E. coli* and purified by affinity chromatography (Fig. S3),
142 whereas the full-length BmNag31 lacking the MBP tag was difficult to obtain due to the
143 protein's insolubility. Therefore, MBP-BmNag31 and BmGH31 were used for this study. The
144 calculated molecular masses of MBP-BmNag31 and BmGH31 (based on the amino acid
145 sequences) are 166 and 106 kDa, respectively. However, the molecular mass of BmGH31 as
146 determined by gel filtration is 655 kDa, suggesting that BmGH31 forms a hexamer in buffer
147 solution (Figs. 3A and S4). MBP-BmNag31 eluted at a point lower than the highest molecular
148 weight marker protein (thyroglobulin, 660 kDa), thus the molecular weight of MBP-BmNag31
149 could not be determined accurately but was estimated to be more than 787 kDa. Moreover, the
150 blue native PAGE analysis supported the hexameric state based on the result of gel filtration
151 chromatography (Fig. 3B). In the case of the catalytic domain of EfNag31A (EfGH31), gel
152 filtration results suggest that the molecular masses of its forms with and without the CBM32
153 domain (theoretical molecular weights = 122 kDa and 107 kDa, respectively) are 117 and 99.7
154 kDa, respectively, indicating that EfGH31 is monomeric.

155

156 **Kinetic analysis and substrate specificity**

157 The hydrolytic activities of both MBP-BmNag31 and BmGH31 were tested against various
158 *para*-nitrophenyl (pNP) glycosides. The enzymes hydrolyzed *p*-nitrophenyl *N*-acetyl- α -D-
159 galactosaminide (GalNAc α -pNP) but not GlcNAc- β -1,3-GalNAc α -pNP and the other substrate,
160 indicating that BmNag31 is an *exo*-acting α GalNAcase, which matches the activity of its
161 bacterial homologs (Cao et al., 2020; Rahfeld et al., 2019). In addition, BmGH31 was active
162 toward bovine submaxillary mucin (Fig. S5) whereas blood type A antigen triaose (GalNAc α 1-
163 3(Fuc α 1-2)Gal) and Tn antigen (GalNAc α -Ser) were not hydrolyzed by the enzyme (data not
164 shown). The k_{cat} values of MBP-BmNag31 and BmGH31 against GalNAc α -pNP are $3.23 \pm$
165 0.10 and 4.81 ± 0.11 s⁻¹, respectively; while their K_m values are 610 ± 10 and 440 ± 5 μ M,
166 respectively. Thus, the truncation of CBM32 domain did not significantly affect the hydrolytic
167 activity of BmNag31. The k_{cat}/K_m values of BmNag31 are 3–8 times lower than that of the
168 Nag31 bacterial homologs due to the latter's relatively high K_m values (Table 1). For both

169 recombinant enzymes, the optimum pH and temperature for the hydrolysis of GalNAc α -pNP
170 were 6.0–6.5 and 45°C–50°C, respectively. Both recombinant enzymes were stable (>90%
171 residual activity) at pH values ranging from 4 to 10 at 4°C for 20 hours. Similarly, they were
172 stable up to 45°C after 30 minutes of incubation (Fig. S6).

173

174 **Binding activity of BmCBM32 toward monosaccharides**

175 The binding activities of a carbohydrate-binding module family 32 (CBM32) domain
176 (BmCBM32) and a CBM32 domain of EfNag31A (EfCBM32) toward GalNAc, D-galactose,
177 L-fucose, and *N*-acetylglucosamine (GlcNAc) were examined by ITC. BmCBM32 and
178 EfCBM32 bound GalNAc, with association constants (K_a) of $260 \pm 11.9 \text{ M}^{-1}$ and 266 ± 24.6
179 M^{-1} , respectively (Fig. 4 and Table 2). Both proteins did not bind to the other sugars tested (Fig.
180 4). The K_a value of BmCBM32 is 10 times lower than the values reported for CBM32s shown
181 in Table 2 (Ficko-Blean and Boraston, 2009, 2006; Grondin et al., 2017), except for CpCBM32-
182 1 (Table 2). Compared to various characterized CBM32s, the amino acid sequences of
183 BmCBM32 and EfCBM32 match most closely with CBM32-1 from *Clostridium perfringens*
184 (CpCBM32-1) (26.1% for EfCBM32 and 25.2% for BmCBM32). In summary, our results
185 indicate that the binding activity of BmCBM32 to GalNAc is almost the same as EfCBM32 and
186 is similar to CpCBM32-1, consistent with their sequence homology.

187

188 **Homology models of BmGH31 and BmCBM32**

189 Using the structure of EfGH31 as a template, we used the SWISS-MODEL server to
190 model the BmGH31 structure. EfGH31 consists of the following five domains: N-domain (β -
191 sandwich), catalytic A-domain ($(\beta/\alpha)_8$ barrel), proximal C-domain (β -sandwich), distal C-
192 domain (β -sandwich), and FN3 domain. The A'-subdomain is inserted within the A-domain
193 (Cao et al., 2020). The homology model of BmGH31 shows the same domain architecture as
194 EfGH31 (Fig. 5A). In contrast to the domain architecture, the surface electrostatic potentials
195 differ significantly between BmGH31 and EfGH31 (Fig. 5B and C). The electrostatic potentials
196 of the A-, N-, and proximal C-domains lying on the same side as the active site are all positively
197 charged on BmGH31. This electron bias is absent in the corresponding area of EfGH31. On the
198 opposite side the protein, most of the surface area is either positively charged or non-charged

199 in EfGH31. In contrast, many negatively charged residues are present in the corresponding area
200 of BmGH31 (Fig. 5B). Because surface electrostatic potential is an important factor
201 determining oligomerization (Ali and Imperiali, 2005), this electron potential bias of protein
202 surface may explain the difference between the oligomeric states of EfNag31A and BmNag31.

203 The catalytic residues, Asp407 and Asp460, in the A-domain are configured such that they
204 can interact with GalNAc in the substrate-binding pocket (Fig. 6A). The residues interacting
205 with GalNAc except for Val444 are structurally conserved between BmGH31 and EfGH31.
206 This observation supports the strict specificity for α -N-acetylgalactosaminide substrate. The
207 homology model of BmCBM32 was also constructed by the SWISS-MODEL server using the
208 crystal structure of CpCBM32-1, a domain of *C. perfringens* putative Nag31 (Grondin et al.,
209 2017). Although the structure of CpCBM32-1 in complex with GalNAc was not determined,
210 13 amino acid residues were identified as candidate amino acid residues involved in GalNAc
211 recognition based on nuclear magnetic resonance spectroscopy (Grondin et al., 2017). The
212 amino acid residues involved in binding in CBM32 proteins are diverse and difficult to predict
213 from their primary structure due to their low sequence homology (Fig. S7). Superimposition of
214 the homology models and the crystal structures indicates that only three amino acid residues
215 corresponding to His990, Asn1022, and Phe1085 in CpCBM32-1 were conserved in
216 BmCBM32 and EfCBM32 (Fig. 6B). Compared with another domain CpCBM32-3 of *C.*
217 *perfringens* Nag31 in complex with GalNAc, only two residues, His961 and Asn1003, of
218 BmCBM32 are conserved but Phe1059 is substituted to tyrosine in CpCBM32-3.

219

220 Discussion

221 This study demonstrates the hydrolytic activity of BmNag31 toward GalNAc α -pNP with
222 similar efficiency as the homolog EfNag31A, supported by conservation of the active site
223 residues identified by the primary sequence alignment and the structural homology modeling.
224 In contrast, the BmCBM32 showed the affinity toward GalNAc that is similar to those of
225 EfCBM32 and CpCBM32-1 but is lower than those of CpCBM32-2 and the other GalNAc-
226 recognizing CBM32 proteins. The variety in residues involved in GalNAc-binding may cause
227 the difference of binding affinity to GalNAc. These results indicate that *BmNag31* encodes a
228 functional protein with similar characters as EfNag31A.

229 One notable difference between BmNag31 and EfNag31A is the oligomeric state of the
230 former, which was observed for both recombinant MBP-BmNag31 and BmGH31 proteins. This
231 observation indicates that the C-terminal CBM32 domain is not necessary for hexamer
232 formation and the addition of the N-terminal MBP tag (42.5 kDa) does not affect
233 oligomerization. Therefore, the N terminus probably locates on the surface of the hexamer.
234 Three prokaryotic GH31 enzymes, α -xylosidase YicI from *E. coli* (Lovering et al., 2005), α -
235 glucosidase MalA from *Sulfolobus solfataricus* (Ernst et al., 2006), and α -glucosidase from
236 *Bacillus thermoamyloliquefaciens* (Kashiwabara et al., 2000), exist in hexameric form. YicI is
237 a dimer consisting of trimers and MalA is a trimer consisting of dimers. Both form a cage-like
238 hexamer in which the active sites face the inner side of the hexamer. One possible contribution
239 of the hexamerization is protein stabilization (Ali and Imperiali, 2005). Another one is that the
240 multiple CBM32 domains would make BmNag31 stay in the vicinity of GalNAc-exposed O-
241 glycoprotein substrates. Details on the hexamer structure of BmNag31 will require further
242 investigation using X-ray crystallography, small-angle X-ray scattering, and cryo-electron
243 microscopy.

244 The Nag31s (BcGH31 and BpGH31) in bacteria isolated from human feces work with
245 other carbohydrate-active enzymes in cleaving peptide-linked GalNAc for uptake (Rahfeld et
246 al., 2019). The lumen of the mammalian intestine is covered by a highly developed mucosal
247 layer that is mainly composed of mucins, i.e., heterologous O-GalNAc glycans attached to
248 proteins (Bergstrom and Xia, 2013). O-GalNAc glycans are also present in insects, where they
249 are structurally less complex than their mammalian counterpart, but are essential in many
250 biological processes (Li et al., 2020; Walski et al., 2017). In *B. mori*, N-
251 acetylgalactosaminyltransferase transfers GalNAc from uridine diphosphate GalNAc to a
252 specific residue of a polypeptide in the Golgi apparatus during the first step of O-glycosylation.
253 The enzyme has been identified and biochemically characterized previously (Xu et al., 2018);
254 however, many aspects of O-glycosylation in insects are still unclear.

255 Here, we reveal that the expression level of *BmNag31* increases during the pupal stage
256 and then decreases at the adult stage, suggesting that the transcription level of *BmNag31* might
257 be controlled by transcription factors related to pupation. When the silkworm transforms from
258 larva to pupa, its organs are reconstructed dynamically. One possible biological role of

259 BmNag31 is the degradation of peptide-linked *O*-glycans. In pupation, cell components are
260 degraded by lysosomal enzymes during phagocytosis or the fusion of autophagosomes with
261 lysosomes (Tettamanti and Casartelli, 2019). The pH-optimum of lysosomal enzymes is usually
262 acidic (Winchester, 2005), but the optimum pH of BmNag31 is 6–6.5, and its hydrolytic activity
263 decreased by 50% in a pH 5 buffer solution. Moreover, BmNag31 has no signal sequence
264 related to transportation to the endoplasmic reticulum. To our knowledge, α -*N*-
265 acetylgalactosaminidase from other insects have not been reported, but insects including *B.*
266 *mori* have genes for proteins belonging to the GH27 family, which contains vertebrate
267 lysosomal α GalNAcase (Wang et al., 1990). Further investigation will be required to reveal the
268 activity of these proteins and their relationship in insects.

269 In conclusion, *BmNag31* is remarkably expressed during the pupal stage of *B. mori* and
270 encodes a functional α GalNAcase with the CBM32 domain that showed affinity toward
271 GalNAc. Furthermore, considering together with the fact that Nag31 homologs are widely
272 distributed among lepidopteran insects, Nag31 proteins may play a role mainly in pupation
273 process. This is the first report of a eukaryotic GH31 α GalNAcase and a eukaryotic hexameric
274 GH31 enzyme and will contribute to understanding the metabolism of carbohydrates in
275 Lepidoptera.

276

277

278 **Experimental Procedures**

279

280 **Chemicals and strains**

281 *p*-Nitrophenyl α -D-galactopyranoside, *p*-nitrophenyl β -D-fucopyranoside, *p*-
282 nitrophenyl β -D-glucuronide, *p*-nitrophenyl β -D-xylopyranoside, *p*-nitrophenyl β -cellobioside,
283 and GlcNAc- β -1,3-GalNAc- α -pNP were purchased from Tokyo Chemical Industry Co., Ltd.
284 (Tokyo, Japan). *p*-Nitrophenyl α -L-fucopyranoside, *p*-nitrophenyl α -D-glucopyranoside, *p*-
285 nitrophenyl *N*-acetyl- β -D-glucosaminide, *p*-nitrophenyl *N*-acetyl- β -D-galactosaminide, *p*-
286 nitrophenyl α -D-mannopyranoside were from Merck (Darmstadt, Germany). *N*-
287 Acetylgalactosamine, *p*-nitrophenyl β -D-glucopyranoside, and *p*-nitrophenyl β -D-
288 galactopyranoside were from FUJIFILM Wako Pure Chemical Co. (Osaka, Japan). *p*-

289 Nitrophenyl *N*-acetyl- α -D-glucopyranoside, *p*-nitrophenyl α -L-rhamnopyranoside, and *p*-
290 nitrophenyl α -D-xylopyranoside were from Carbosynth (Berksher, UK). Fucose and galactose
291 were from Nacalai Tesque (Kyoto, Japan). *p*-Nitrophenyl β -D-mannopyranoside (Megazyme
292 USA), GalNAc α -pNP (Cayman Chemical, Michigan, USA), blood type A antigen triaose
293 (Elicityl, Crolles, France), and Tn antigen (Dextra Laboratories Ltd., Thames Valley Science
294 Park, UK) were also used in this study. Silkworms (*B. mori* F1 hybrid Fuyo \times Tsukubane)
295 purchased from Ehime Sanshu Inc. (Ehime, Japan) were raised on an artificial diet, Silkmate
296 S2 (Nohsan Corporation, Yokohama, Japan), in an incubator at 25°C.

297

298 **In silico analysis**

299 Using the amino acid sequence of BmNag31 from SilkBase ([http://silkbase.ab.a.u-](http://silkbase.ab.a.u-tokyo.ac.jp/cgi-bin/index.cgi)
300 [tokyo.ac.jp/cgi-bin/index.cgi](http://silkbase.ab.a.u-tokyo.ac.jp/cgi-bin/index.cgi)) we searched for similar sequences in the NCBI server
301 (<https://blast.ncbi.nlm.nih.gov/Blast.cgi>) and InsectBase (<http://www.insect-genome.com/>)
302 database (Livak and Schmittgen, 2001). The resulting lepidopteran sequences and the
303 sequence of EfNag31A (GenBank id EOK08638.1) were aligned using the ClustalW program
304 running within MEGA X software (Kumar et al., 2018) and the alignment diagram was
305 generated using ESPript 3.0 (Robert and Gouet, 2014). SignalP 5.0
306 (<http://www.cbs.dtu.dk/services/SignalP/>) was used to predict the location of the signal peptide.
307 Subcellular localization of BmNag31 was predicted by DeepLoc-1.0
308 (<http://www.cbs.dtu.dk/services/DeepLoc>) (Armenteros et al., 2017). Homology models of
309 BmNag31, BmCBM32, and EfCBM32 were generated by the SWISS-MODEL server
310 (<https://swissmodel.expasy.org>) using the coordinate of EfGH31 (PDB 6M77) or the CBM32-
311 1 domain from *Clostridium perfringens* (PDB 4LPL) as a template. The surface electron
312 potential was calculated using the APBD electro-statistics plugin of PyMOL software
313 (<https://pymol.org>).

314

315 **Transcriptional analysis**

316 Day-3 fifth-instar silkworm larvae were dissected; their tissues were washed in
317 phosphate-buffered saline (PBS) and immediately frozen in liquid nitrogen, then stored at
318 -80°C . Total RNA was extracted from the whole body or individual tissues of silkworms using

319 TRIzol reagent (Thermo Fisher Scientific, Waltham, MA, USA), followed by treatment with
320 DNase I (Nippon Gene, Tokyo, Japan). First-strand cDNA was synthesized from 500 ng of
321 RNA using PrimeScript RT reagent kit (Takara Bio, Shiga, Japan). Specific genes were
322 quantified by quantitative PCR (qPCR) using the primers listed in Table S1 and the SYBR
323 Green qPCR reagent (Thermo Fisher Scientific). The expression levels of *BmNag31* were
324 normalized relative to that of the glyceraldehyde-3-phosphate dehydrogenase (*BmGAPDH*)
325 gene (Guo et al., 2016) and the expression ratio of *BmNag31* was calculated by the $2^{-\Delta Ct}$ method
326 (Pfaffl, 2001).

327

328 **Plasmid construction**

329 Genomic DNA of a fifth-instar silkworm larva was extracted using the ISOGENOME
330 (Nippon Gene) genome extraction reagent. The DNA fragment encoding *BmNag31* was
331 amplified from the genomic DNA using the primers *BmGH31_pET21a_F* and
332 *BmGH31_pET21a_R* (Table S1). A pET21a vector (Merck) was linearized by *NdeI* and *XhoI*
333 restriction enzymes and then ligated with the fragment encoding *BmNag31* using the In-Fusion
334 cloning kit (Takara Bio). To construct the plasmid used to express MBP-*BmNag31*, first, the
335 DNA fragment encoding *BmNag31* with a C-terminal hexahistidine tag was amplified using
336 the primer pair *BmGH31_NcoI_F* and *Ct-His6-SalI_R*, and *BmNag31*-harboring pET21a as a
337 template. The amplicons were then ligated into the pMAL-c5x vector (New England Biolabs,
338 Ipswich, MA, USA). We then constructed plasmids expressing *BmGH31* (residues 1–925) and
339 *BmCBM32* domain (residues 926–1069). First, DNA fragments encoding the domains were
340 amplified from plasmid pET21a harboring *BmNag31* using the primer pairs
341 *BmGH31_pET21a_F* and *BmGH31 Δ CBM32_XhoI_R*, and *BmCBM32_NheI_F* and
342 *BmCBM32_XhoI_R*. The resulting amplicons were then ligated into pET28a vectors (Merck)
343 using *NdeI* and *XhoI* restriction sites, and *NheI* and *XhoI* sites, respectively. The expression
344 plasmid for *EfCBM32* (residues 981–1126) was generated by inverse PCR using the
345 *EfNag31A*-harboring pET28a as a template, which was constructed in a previous study
346 (Miyazaki and Park, 2020). The identities of all DNAs were confirmed by sequencing and the
347 nucleotide sequence of *BmNag31* was submitted to the DDBJ/EMBL/GenBank databases with
348 the accession number LC581276.

349

350 **Recombinant expression and purification**

351 *E. coli* BL21 (DE3) harboring the desired plasmid was grown at 37°C to an optical density
352 (600 nm) of 0.6 in 1 L of Luria-Bertani medium containing 50 µg/mL of kanamycin or 50 µg/mL
353 of carbenicillin. After cooling the medium to 20°C on ice, expression was induced by the
354 addition of 0.1 mM IPTG at 20°C for 20 hours. The cells were harvested by centrifugation for
355 10 minutes (4°C 5,000 × g) and stored at –20°C. The cell pellet was resuspended in two types
356 of purification buffers: PBS for MBP-BmNag31 or 50 mM sodium phosphate buffer (pH 8.0)
357 containing 300 mM NaCl and 20 mM imidazole for the other His-tagged proteins. Following
358 resuspension, the cells were disrupted by ultrasonication and then centrifuged to remove
359 insoluble materials. To purify MBP-BmNag31, the supernatant was loaded onto an amylose
360 resin (New England Biolabs) column pre-equilibrated with PBS. The column was then washed
361 with PBS and the protein was eluted with PBS containing 10 mM maltose. Using 30-kDa cutoff
362 Amicon Ultra centrifugal units (Merck), we replaced the purified MBP-BmNag31 buffer with
363 50 mM sodium phosphate buffer (pH 8.0) containing 300 mM NaCl and 20 mM imidazole.
364 Purified MBP-BmNag31, along with other His-tagged proteins in the cell lysate supernatant,
365 were loaded onto a Ni-NTA Agarose (Qiagen, Manchester, UK) column, and the unbound
366 proteins were washed with the same buffer containing 20–50 mM imidazole. Proteins were
367 eluted with the same buffer containing 100 mM imidazole and then concentrated by
368 ultrafiltration using Amicon Ultra centrifugal units and 50 mM sodium phosphate buffer (pH
369 6.5) containing 300 mM NaCl. MBP-BmNag31, BmCBM32, and EfCBM32 were then dialyzed
370 with 50 mM 4-(2-hydroxyethyl)-1-piperazine ethane sulfonic acid (HEPES) buffer (pH 7.0).
371 Protein purity was confirmed by sodium dodecyl sulfate–polyacrylamide gel electrophoresis.
372 Protein concentration was calculated from the absorbance at 280 nm using the theoretical
373 extinction coefficients predicted by the ProtParam tool (<https://web.expasy.org/protparam/>)
374 based on their amino acid sequences.

375

376 **Molecular weight determination**

377 Gel filtration chromatography was performed using the ÄKTA explorer 10S system (GE
378 Healthcare, Chicago, IL, USA). Purified MBP-BmNag31 and BmGH31 were concentrated to

379 5 mg/mL with Amicon Ultra centrifugation filter units, then the concentrated proteins were
380 applied onto a HiLoad 16/60 Superdex 200 prep grade column and eluted by 1.2 column
381 volumes of 20 mM sodium phosphate buffer (pH 7.0) containing 300 mM NaCl. EfNag31A
382 and EfGH31 were also analyzed by gel filtration chromatography according to previously
383 published procedures (Miyazaki and Park, 2020). For blue native PAGE, 1 mg/mL of each
384 protein and marker protein solution (HMW Native Marker Kit, GE Healthcare) were
385 individually mixed with an equal volume of sample buffer [1% (w/v) Coomassie Brilliant Blue
386 G-250, 20 mM 6-aminocaproic acid, 20 mM Bis-Tris-HCl (pH 7.0), 20% (v/v) glycerol] and
387 then incubated on ice for 5 minutes. Ten microliters of each sample was applied on 3%–10%
388 PAGEL native PAGE gels (ATTO, Tokyo, Japan) and electrophoresed using 50 mM Bis-Tris-
389 HCl (pH 7.0) as the anode buffer and 0.02% Coomassie Brilliant Blue G-250, 50 mM Tricine,
390 15 mM Bis-Tris-HCl (pH 7.0) as the cathode buffer. After electrophoresis, the gel was destained
391 using a 25% methanol–7.5% acetic acid solution.

392

393 **Enzyme assays**

394 Hydrolytic activity toward various *p*-nitrophenyl glycosides was measured in 50 μ L
395 reaction mixtures containing 25.6 μ g/mL MBP-BmNag31 or 12.8 μ g/mL BmGH31, 1 mM of a
396 substrate, and 20 mM sodium phosphate buffer (pH 7.0) at 30°C. To examine the effect of pH
397 on hydrolytic activity, reaction mixtures containing 11 μ g/mL of MBP-BmNag31 or 6.4 μ g/mL
398 BmGH31 and 1 mM GalNAc α -pNP were prepared with McIlvaine (sodium citrate–phosphate)
399 buffer at pH 4.0–8.0 or in glycine-HCl buffer at pH 9.0–10. The mixtures were incubated for
400 10 min at 30°C. The effect of temperature on hydrolytic activity was examined using 50 mM
401 sodium phosphate buffer (pH 6.5) containing 100 mM NaCl and 1 mM GalNAc α -pNP.
402 Mixtures were incubated at temperatures ranging from 20°C–60°C. We tested the enzymes' pH
403 stability by incubating 400 μ g/mL of both enzymes for 20 hours in McIlvaine buffer (pH 4.0–
404 8.0) or glycine-HCl buffer (pH 9.0–10). We tested the enzymes' thermal stability by incubating
405 150 μ g/mL of MBP-BmNag31 and 150 μ g/mL of BmGH31 at 4°C–60°C for 30 minutes in 50
406 mM sodium phosphate buffer containing 300 mM NaCl (pH 6.5). The residual activities for pH
407 stability and thermostability were measured at 30°C with the reaction mixtures containing 9
408 μ g/mL and 15 μ g/mL of each protein, respectively, and 50 mM sodium phosphate buffer (pH

409 7.0) containing 1 mM of GalNAc α -pNP. The mixtures were incubated at 30°C for experiments
410 testing pH stability and for thermostability. The initial hydrolytic reaction velocities of
411 GalNAc α -pNP were determined using 50 mM sodium phosphate buffer (pH 6.0) containing
412 five concentrations (0.1–2.0 mM) of GalNAc α -pNP at 40°C. All reactions above were
413 performed in triplicate and quenched by adding 100 μ L of 1 M Na₂CO₃. The amount of released
414 *p*-nitrophenol was measured at 405 nm. Kinetic parameters were calculated by fitting to the
415 Michaelis–Menten equation using nonlinear regression analysis by KaleidaGraph software
416 (Synergy Software, Reading PA, USA). The hydrolytic activity of the enzymes toward blood
417 group A antigen triaose was evaluated in 10- μ L reaction mixtures containing 10 mM of the
418 oligosaccharide and 150 μ g/mL of BmGH31 in 50 mM sodium phosphate buffer (pH 7.0). For
419 the Tn antigen, the reaction mixture contained 6 mM Tn antigen and 100 μ g/mL of BmGH31
420 or EfGH31. All reaction mixtures were incubated at 30°C overnight, followed by thin-layer
421 chromatography (TLC) using TLC Silica Gel 60 F₂₅₄ TLC plates (Merck). To visualize the
422 carbohydrates, the TLC plate was sprayed with 10% sulfuric acid in methanol and then baked.
423 5 mg of mucin from bovine submaxillary gland (Merck) was pre-treated with 250 units/mL of
424 *Clostridium perfringens* neuraminidase, 25 units/mL of *Streptomyces plicatus* β -*N*-
425 acetylhexosaminidase (New England Biolabs), and 25 μ g/mL of *Streptococcus pneumoniae* β -
426 galactosidase 35A (NZYTech, Lisbon, Portugal) in 1 mL of reaction mixture for 20 hours at
427 30 °C, and then the reaction mixture was concentrated by centrifugal evaporation and the mucin
428 was precipitated twice with 80% ethanol to remove the released sugars. The precipitate was
429 dissolved in water and incubated with BmGH31 for 20 hours at 30 °C. The reaction mixture
430 was mixed with four volumes of ethanol, followed by centrifugation to remove proteins, and
431 then supernatant was concentrated by centrifugal evaporation. Reaction products were analyzed
432 by TLC and developed in a mixture of 1-butanol/acetic acid/water (2 : 1 : 1 by volume).
433 Released sugars were visualized using diphenylamine/aniline/phosphoric acid reagent
434 (Anderson et al., 2000).

435

436 **Isothermal titration calorimetry**

437 The binding affinities of CBM32 domains toward GalNAc, D-galactose, L-fucose, and
438 GlcNAc were analyzed by isothermal titration calorimetry (ITC) using a MicroCal iTC200

439 (Malvern Panalytical Ltd, Enigma Business Park, UK). BmCBM32 and EfCBM32 were
440 dialyzed against 50 mM HEPES buffer (pH 7.0) and filtered using 0.45 µm filters (Merck).
441 Titrations were performed at 25°C by injecting 2 µL aliquots of 10 mM ligand dissolved in the
442 50 mM HEPES buffer (pH 7.0) into a cell containing 0.1 mM CBM32 protein. The resulting
443 heat release was recorded and the titration data were analyzed using MicroCal Origin ITC
444 software (Malvern Panalytical Ltd). Thermodynamic parameters were obtained by nonlinear
445 least-squares fitting of experimental data using the one set sites binding model.

446

447 **Author contributions**

448 TM conceived and supervised the study; MI and TM performed experiments; all authors
449 analyzed the data; MI and TM wrote and revised the manuscript; all authors read and approved
450 the manuscript.

451

452 **References**

- 453 Aga, H., Maruta, K., Yamamoto, T., Kubota, M., Fukuda, S., Kurimoto, M., Tsujisaka, Y.,
454 (2002) Cloning and Sequencing of the Genes Encoding Cyclic Tetrasaccharide-
455 synthesizing Enzymes from *Bacillus globisporus* C11. *Bioscience, Biotechnology,*
456 *and Biochemistry*, **66**, 1057–1068. <https://doi.org/10.1271/bbb.66.1057>
- 457 Anderson, K., Li, S., Li, Y., (2000) Diphenylamine–Aniline–Phosphoric Acid Reagent, a
458 Versatile Spray Reagent for Revealing Glycoconjugates on Thin-Layer
459 Chromatography Plates. *Analytical Biochemistry*, **287**, 337–339,
460 <https://doi.org/10.1006/abio.2000.4829>
- 461 Armenteros, J.J.A., Sønderby, C. K., Sønderby, S. K., Nielsen, H., Winther, O., (2017)
462 DeepLoc: prediction of protein subcellular localization using deep learning.
463 *Bioinformatics*, **33**, 3387–3395. <https://doi.org/10.1093/bioinformatics/btx431>
- 464 Ali, M.H., Imperiali, B., (2005) Protein oligomerization: How and why. *Bioorganic &*
465 *Medicinal Chemistry*, **13**, 5013–5020. <https://doi.org/10.1016/j.bmc.2005.05.037>
- 466 Bergstrom, K.S.B., Xia, L., (2013) Mucin-type O-glycans and their roles in intestinal
467 homeostasis. *Glycobiology*, **23**, 1026–1037. <https://doi.org/10.1093/glycob/cwt045>
- 468 Cao, H., Walton, J.D., Brumm, P., Phillips, G.N., (2020) Crystal structure of α-xylosidase
469 from *Aspergillus niger* in complex with a hydrolyzed xyloglucan product and new
470 insights in accurately predicting substrate specificities of GH31 family glycosidases.
471 *ACS Sustainable Chemistry and Engineering*, **8**, 2540–2547.
472 <https://doi.org/10.1021/acssuschemeng.9b07073>

- 473 Chen, B., Yu, T., Xie, S., Du, K., Liang, X., Lan, Y., Sun, C., Lu, X., Shao, Y., (2018)
474 Comparative shotgun metagenomic data of the silkworm *Bombyx mori* gut
475 microbiome. *Scientific Data*, **5**, 180285. <https://doi.org/10.1038/sdata.2018.285>
- 476 Daimon, T., Hamada, K., Mita, K., Okano, K., Suzuki, M.G., Kobayashi, M., Shimada, T.,
477 (2003) A *Bombyx mori* gene, *BmChi-h*, encodes a protein homologous to bacterial
478 and baculovirus chitinases. *Insect Biochemistry and Molecular Biology*, **33**, 749–759.
479 [https://doi.org/10.1016/S0965-1748\(03\)00084-5](https://doi.org/10.1016/S0965-1748(03)00084-5)
- 480 Daimon, T., Taguchi, T., Meng, Y., Katsuma, S., Mita, K., Shimada, T., (2008) β -
481 Fructofuranosidase genes of the silkworm, *Bombyx mori*: Insights into enzymatic
482 adaptation of *B. mori* to toxic alkaloids in mulberry latex. *Journal of Biological*
483 *Chemistry*, **283**, 15271–15279. <https://doi.org/10.1074/jbc.M709350200>
- 484 D’Alessio, C., M. Dahms, N., (2015) Glucosidase II and MRH-Domain Containing
485 Proteins in the Secretory Pathway. *Current Protein & Peptide Science*, **16**, 31–48.
486 <https://doi.org/10.2174/1389203716666150213160438>
- 487 Ernst, H.A., lo Leggio, L., Willemoës, M., Leonard, G., Blum, P., Larsen, S., (2006)
488 Structure of the *Sulfolobus solfataricus* α -Glucosidase: Implications for Domain
489 Conservation and Substrate Recognition in GH31. *Journal of Molecular Biology*, **358**,
490 1106–1124. <https://doi.org/10.1016/j.jmb.2006.02.056>
- 491 Ficko-Blean, E., Boraston, A.B., (2009) *N*-Acetylglucosamine Recognition by a Family
492 32 Carbohydrate-Binding Module from *Clostridium perfringens* NagH. *Journal of*
493 *Molecular Biology*, **390**, 208–220. <https://doi.org/10.1016/j.jmb.2009.04.066>
- 494 Ficko-Blean, E., Boraston, A.B., (2006) The Interaction of a Carbohydrate-binding
495 Module from a *Clostridium perfringens* *N*-Acetyl- β -hexosaminidase with Its
496 Carbohydrate Receptor. *Journal of Biological Chemistry*, **281**, 37748–37757.
497 <https://doi.org/10.1074/jbc.M606126200>
- 498 Goldsmith, M.R., Shimada, T., Abe, H., (2005) The genetics and genomics of the silkworm,
499 *Bombyx mori*. *Annual Review of Entomology*, **50**, 71–100.
500 <https://doi.org/10.1146/annurev.ento.50.071803.130456>
- 501 Grondin, J.M., Duan, D., Kirlin, A.C., Abe, K.T., Chitayat, S., Spencer, H.L., Spencer, C.,
502 Campigotto, A., Houlston, S., Arrowsmith, C.H., Allingham, J.S., Boraston, A.B.,
503 Smith, S.P., (2017) Diverse modes of galacto-specific carbohydrate recognition by a
504 family 31 glycoside hydrolase from *Clostridium perfringens*. *PLoS ONE*, **12**.
505 <https://doi.org/10.1371/journal.pone.0171606>
- 506 Guo, H., Jiang, L., Xia, Q., (2016) Selection of reference genes for analysis of stress-
507 responsive genes after challenge with viruses and temperature changes in the
508 silkworm *Bombyx mori*. *Molecular Genetics and Genomics*, **291**, 999–1004.
509 <https://doi.org/10.1007/s00438-015-1125-4>
- 510 Kashiwabara, S., Azuma, S., TsudukiI, M., Suzuki, Y., (2000) The Primary Structure of the

511 Subunit in *Bacillus thermoamyloliquefaciens* KP1071 Molecular Weight 540,000
512 Homohexameric α -Glucosidase II Belonging to the Glycosyl Hydrolase Family 31.
513 *Bioscience, Biotechnology, and Biochemistry*, **64**, 1379–1393.
514 <https://doi.org/10.1271/bbb.64.1379>

515 Kawahara, A.Y., Plotkin, D., Espeland, M., Meusemann, K., Toussaint, E.F.A., Donath, A.,
516 Gimmich, F., Frandsen, P.B., Zwick, A., dos Reis, M., Barber, J.R., Peters, R.S., Liu,
517 S., Zhou, X., Mayer, C., Podsiadlowski, L., Storer, C., Yack, J.E., Misof, B., Breinholt,
518 J.W., (2019) Phylogenomics reveals the evolutionary timing and pattern of butterflies
519 and moths. *Proceedings of the National Academy of Sciences of the United States of*
520 *America*, **116**, 22657–22663. <https://doi.org/10.1073/pnas.1907847116>

521 Kawamoto, M., Jouraku, A., Toyoda, A., Yokoi, K., Minakuchi, Y., Katsuma, S., Fujiyama,
522 A., Kiuchi, T., Yamamoto, K., Shimada, T., (2019) High-quality genome assembly of
523 the silkworm, *Bombyx mori*. *Insect Biochemistry and Molecular Biology*, **107**, 53–62.
524 <https://doi.org/10.1016/j.ibmb.2019.02.002>

525 King, B.R., Vural, S., Pandey, S., Barteau, A., Guda, C., (2012) ngLOC: software and web
526 server for predicting protein subcellular localization in prokaryotes and eukaryotes.
527 *BMC Research Notes*, **5**, 351. <https://doi.org/10.1186/1756-0500-5-351>

528 Kumar, S., Stecher, G., Li, M., Knyaz, C., Tamura, K., (2018) MEGA X: Molecular
529 Evolutionary Genetics Analysis across Computing Platforms. *Molecular Biology and*
530 *Evolution*, **35**, 1547–1549. <https://doi.org/10.1093/molbev/msy096>

531 Li, W., de Schutter, K., van Damme, E.J.M., Smagghe, G., (2020) Synthesis and biological
532 roles of O-glycans in insects. *Glycoconjugate Journal*, **37**, 47–56.
533 <https://doi.org/10.1007/s10719-019-09867-1>

534 Li, Z.W., Shen, Y.H., Xiang, Z.H., Zhang, Z., (2011) Pathogen-origin horizontally
535 transferred genes contribute to the evolution of Lepidopteran insects. *BMC*
536 *Evolutionary Biology*, **11**, 356. <https://doi.org/10.1186/1471-2148-11-356>

537 Liu, T., Chen, L., Zhou, Y., Jiang, X., Duan, Y., Yang, Q., (2017) Structure, catalysis, and
538 inhibition of OfChi-h, the lepidoptera-exclusive insect chitinase. *Journal of*
539 *Biological Chemistry*, **292**, 2080–2088. <https://doi.org/10.1074/jbc.M116.755330>

540 Livak, K.J., Schmittgen, T.D., (2001) Analysis of relative gene expression data using real-
541 time quantitative PCR and the $2^{-\Delta\Delta C_T}$ method. *Methods*, **25**, 402–408.
542 <https://doi.org/10.1006/meth.2001.1262>

543 Lombard, V., Golaconda Ramulu, H., Drula, E., Coutinho, P.M., Henrissat, B., (2014) The
544 carbohydrate-active enzymes database (CAZy) in 2013. *Nucleic Acids Research*, **42**,
545 D490–D495. <https://doi.org/10.1093/nar/gkt1178>

546 Lovering, A.L., Lee, S.S., Kim, Y.-W., Withers, S.G., Strynadka, N.C.J., (2005)
547 Mechanistic and Structural Analysis of a Family 31 α -Glucosidase and Its Glycosyl-
548 enzyme Intermediate. *Journal of Biological Chemistry*, **280**, 2105–2115.

549 <https://doi.org/10.1074/jbc.M410468200>
550 Lu, F., Wei, Z., Luo, Y., Guo, H., Zhang, G., Xia, Q., Wang, Y., (2020) SilkDB 3.0:
551 Visualizing and exploring multiple levels of data for silkworm. *Nucleic Acids*
552 *Research*, **48**, D749–D755. <https://doi.org/10.1093/nar/gkz919>
553 Miyazaki, T., Park, E.Y., (2020) Crystal structure of the *Enterococcus faecalis* α -N-
554 acetylgalactosaminidase, a member of the glycoside hydrolase family 31. *FEBS*
555 *Letters*, **594**, 2282–2293. <https://doi.org/10.1002/1873-3468.13804>
556 Miyazaki T., Oba N., Park. E.Y., (2020) Structural insight into the substrate specificity of
557 *Bombyx mori* β -fructofuranosidase belonging to the glycoside hydrolase family 32.
558 *Insect biochemistry Molecular Biology*, **127**, 103494
559 Pfaffl, M.W., (2001) A new mathematical model for relative quantification in real-time RT-
560 PCR. *Nucleic Acids Research*, **29**, 45e–445. <https://doi.org/10.1093/nar/29.9.e45>
561 Qin, J., Li, R., Raes, J., Arumugam, M., Burgdorf, K.S., Manichanh, C., Nielsen, T., Pons,
562 N., Levenez, F., Yamada, T., Mende, D.R., Li, J., Xu, J., Li, Shaochuan, Li, D., Cao,
563 J., Wang, B., Liang, H., Zheng, H., Xie, Y., Tap, J., Lepage, P., Bertalan, M., Batto,
564 J.-M., Hansen, T., le Paslier, D., Linneberg, A., Nielsen, H.B., Pelletier, E., Renault,
565 P., Sicheritz-Ponten, T., Turner, K., Zhu, H., Yu, C., Li, Shengting, Jian, M., Zhou, Y.,
566 Li, Y., Zhang, X., Li, Songgang, Qin, N., Yang, H., Wang, Jian, Brunak, S., Doré, J.,
567 Guarner, F., Kristiansen, K., Pedersen, O., Parkhill, J., Weissenbach, J., Bork, P.,
568 Ehrlich, S.D., Wang, Jun, (2010) A human gut microbial gene catalogue established
569 by metagenomic sequencing. *Nature*, **464**, 59–65.
570 <https://doi.org/10.1038/nature08821>
571 Rahfeld, P., Wardman, J.F., Mehr, K., Huff, D., Morgan-Lang, C., Chen, H.-M., Hallam,
572 S.J., Withers, S.G., (2019) Prospecting for microbial α -N-acetylgalactosaminidases
573 yields a new class of GH31 O-glycanase. *Journal of Biological Chemistry*, **294**,
574 16400–16415. <https://doi.org/10.1074/jbc.RA119.010628>
575 Robert, X., Gouet, P., (2014) Deciphering key features in protein structures with the new
576 ENDscript server. *Nucleic Acids Research*, **42**, W320–W324.
577 <https://doi.org/10.1093/nar/gku316>
578 Roig-Zamboni, V., Cobucci-Ponzano, B., Iacono, R., Ferrara, M.C., Germany, S., Bourne,
579 Y., Parenti, G., Moracci, M., Sulzenbacher, G., (2017) Structure of human lysosomal
580 acid α -glucosidase—a guide for the treatment of Pompe disease. *Nature*
581 *Communications*, **8**, 1111. <https://doi.org/10.1038/s41467-017-01263-3>
582 Rozeboom, H.J., Yu, S., Madrid, S., Kalk, K.H., Zhang, R., Dijkstra, B.W., (2013) Crystal
583 structure of α -1,4-Glucan lyase, a unique glycoside hydrolase family member with a
584 novel catalytic mechanism. *Journal of Biological Chemistry*, **288**, 26764–26774.
585 <https://doi.org/10.1074/jbc.M113.485896>
586 Sieber, K.B., Bromley, R.E., Dunning Hotopp, J.C., (2017) Lateral gene transfer between

587 prokaryotes and eukaryotes. *Experimental Cell Research*, **358**, 421–426.
588 <https://doi.org/10.1016/j.yexcr.2017.02.009>

589 Sun, B.F., Xiao, J.H., He, S.M., Liu, L., Murphy, R.W., Huang, D.W., (2013) Multiple
590 ancient horizontal gene transfers and duplications in lepidopteran species. *Insect*
591 *Molecular Biology*, **22**, 72–87. <https://doi.org/10.1111/imb.12004>

592 Tettamanti, G., Casartelli, M., (2019) Cell death during complete metamorphosis.
593 *Philosophical Transactions of the Royal Society B: Biological Sciences*, **374**,
594 20190065. <https://doi.org/10.1098/rstb.2019.0065>

595 Walski, T., de Schutter, K., van Damme, E.J.M., Smagghe, G., (2017) Diversity and
596 functions of protein glycosylation in insects. *Insect Biochemistry and Molecular*
597 *Biology*, **83**, 21–34. <https://doi.org/10.1016/j.ibmb.2017.02.005>

598 Wang, A. M., Bishop, D. F., Desnick, R. J., (1990) Human alpha-N-
599 acetylgalactosaminidase-molecular cloning, nucleotide sequence, and expression of
600 a full-length cDNA. Homology with human alpha-galactosidase A suggests evolution
601 from a common ancestral gene. *Journal of Biological Chemistry*, **265**, 21859–21866,
602 [https://doi.org/10.1016/S0021-9258\(18\)45818-8](https://doi.org/10.1016/S0021-9258(18)45818-8)

603 Wang, C. -F., Sun, W., Zhang, Z., (2019) Functional characterization of the horizontally
604 transferred 4,5-DOPA extradiol dioxygenase gene in the domestic silkworm, *Bombyx*
605 *mori*. *Insect Molecular Biology*, **28**, 409–419. <https://doi.org/10.1111/imb.12558>

606 Watanabe, S., Kakudo, A., Ohta, M., Mita, K., Fujiyama, K., Inumaru, S., (2013)
607 Molecular cloning and characterization of the α -glucosidase II from *Bombyx mori*
608 and *Spodoptera frugiperda*, *Insect Biochemistry and Molecular Biology*, **43**, 319–327,
609 <https://doi.org/10.1016/j.ibmb.2013.01.005>

610 Wheeler, D., Redding, A.J., Werren, J.H., (2013) Characterization of an Ancient
611 Lepidopteran Lateral Gene Transfer. *PLoS ONE*, **8**, e59262.
612 <https://doi.org/10.1371/journal.pone.0059262>

613 Winchester, B., (2005) Lysosomal metabolism of glycoproteins. *Glycobiology*, **15**, 1R–15R.
614 <https://doi.org/10.1093/glycob/cwi041>

615 Xu, J., Morio, A., Morokuma, D., Nagata, Y., Hino, M., Masuda, A., Li, Z., Mon, H.,
616 Kusakabe, T., Lee, J.M., (2018) A functional polypeptide N-
617 acetylgalactosaminyltransferase (PGANT) initiates O-glycosylation in cultured
618 silkworm BmN4 cells. *Applied Microbiology and Biotechnology*, **102**, 8783–8797.
619 <https://doi.org/10.1007/s00253-018-9309-6>

620 Zhu, B., Lou, M.M., Xie, G.L., Zhang, G.Q., Zhou, X.P., Li, B., Jin, G.L., (2011)
621 Horizontal gene transfer in silkworm, *Bombyx mori*. *BMC Genomics*, **12**, 248.
622 <https://doi.org/10.1186/1471-2164-12-248>

623

624 **Table 1. Kinetic parameters for the hydrolysis of GalNAc α -pNP by BmNag31**
 625 **recombinant enzymes and related enzymes.**

Enzyme	k_{cat} (s ⁻¹)	K_m (μ M)	k_{cat}/K_m (s ⁻¹ mM ⁻¹)	Reference
MBP-BmNag31	3.23 \pm 0.10	610 \pm 10	5.30	This study
BmGH31	4.81 \pm 0.11	440 \pm 5	10.8	This study
EfGH31-CBM32 ^a	4.45 \pm 0.04	136 \pm 6	33	(Miyazaki and Park, 2020)
EfGH31 ^b	6.54 \pm 0.12	158 \pm 12	41	(Miyazaki and Park, 2020)
BcGH31 ^c	3.6 \pm 0.2	110 \pm 10	32 \pm 4	(Rahfeld et al., 2019)
tBcGH31 ^b	2.1 \pm 0.1	140 \pm 20	16 \pm 2	(Rahfeld et al., 2019)
BpGH31 ^c	7.2 \pm 0.3	270 \pm 20	27 \pm 2	(Rahfeld et al., 2019)
tBpGH31 ^b	2.22 \pm 0.09	140 \pm 20	16 \pm 2	(Rahfeld et al., 2019)

626 ^a Truncated mutant containing the putative GH, FN3, and CBM32 domains.

627 ^b Truncated mutant containing the putative GH and FN3 domains.

628 ^c Full-length enzyme.

629

630

Table 2. Binding affinity of CBM32 proteins toward monosaccharides.

CBM	GH catalytic domain	Sequence identity ^a	K_d (M)	K_a (M ⁻¹)	Ligand	Method	Reference
BmCBM32	GH31	100%		260 ± 11.9	GalNAc	ITC	This study
EfCBM32	GH31	40.8%		266 ± 24.6	GalNAc	ITC	This study
CpCBM32-1	GH31	25.2%	6 ± 2	167^b	GalNAc	NMR	(Grondin et al., 2017)
CpCBM32-2	GH31	20.4%	0.9 ± 0.4	$1 \times 10^3^b$	GalNAc	NMR	(Grondin et al., 2017)
CpCBM32-3	GH31	19.4%	0.9 ± 0.3	$1 \times 10^3^b$	GalNAc	NMR	(Grondin et al., 2017)
CpCBM32	GH84 (CpGH84C)	20.8%		$0.98 (\pm 0.17) \times 10^3$	Galactose	UV difference	(Ficko-Blean and Boraston, 2006)
				$0.86 (\pm 0.12) \times 10^3$	GalNAc	UV difference	(Ficko-Blean and Boraston, 2006)
NagHCBM32-2	GH84 (CpGH84A)	16.5%		$1.88 (\pm 0.02) \times 10^3$	GlcNAc	ITC	(Ficko-Blean and Boraston, 2009)

631 ^aAmino acid sequence identity with BmNag31.632 ^bCalculated from the reported K_d values.

633

634 **Figures**

635

636 **Figure 1. Modular architectures of native and recombinant proteins of BmNag31 and**
637 **EfNag31A.**

638 BmNag31 and EfNag31A refer to the native form of these enzymes, and the other names refer
639 to the recombinant proteins that were expressed in *E. coli* and used in this study. Colors
640 represent the following: signal peptide, *blue*; GH31 catalytic domain, *pale blue*; fibronectin
641 type 3 (FN3) domain, *yellow*; carbohydrate-binding module 32 (CBM32) domain, *green*; Type
642 III cohesin-like domain (COH) and dockerin-like domain (DOC), *gray*; FIVAR domain, *pink*;
643 transmembrane, *purple*; His tag, *orange*; and maltose binding protein (MBP) tag, *light pink*.

644

645 **Figure 2. Expression *BmNag31* gene in different organs and developmental stages.**

646 Relative expression levels of *BmNag31* in each organ in day-3 fifth-instar larvae (A), whole
647 body of first instar larvae to adult stages (B), and midgut from day-3 fifth-instar larvae to day-
648 4 pupae (C) were analyzed using quantitative RT-PCR. The housekeeping gene *BmGAPDH* was
649 used as the internal control. Abbreviations: L1 to L5, first- to fifth-instar larval stages; PP,
650 prepupal stage; P, pupal stage; D, day; W, wandering stage (day-7 fifth-instar larval stage). All
651 experiments were performed in triplicate.

652

653 **Figure 3. Oligomerization analysis of BmNag31.**

654 The oligomeric state of BmNag31 was examined by gel filtration chromatography (A) and blue
655 native PAGE (B). The experimental conditions are described in the Materials and Methods
656 section. (A) Colors and lines of chromatograms are follows: MBP-BmNag31, *blue* line;
657 BmGH31, *red* line; Blue dextran, *gray* line; molecular weight marker, *gray* dashed line. (B) A
658 3%–10 % gradient acrylamide gel was used for blue native PAGE. Lane M, marker; lane 1,
659 MBP-BmNag31; lane 2, BmGH31. MBP-BmNag31 and BmGH31 were highlighted by arrows.

660

661 **Figure 4. Binding activity of CBM32.**

662 Binding activity of BmNag31 (A) and EfNag31A (B) toward GalNAc, D-galactose, GlcNAc,
663 and L-fucose. The results of binding analysis of CBM32 and toward GalNAc show the raw ITC

664 data (upper panels) and integrated heat of binding obtained from the raw data (lower panels).
665 For the other results using D-galactose, GlcNAc, and L-fucose as ligands, only the raw ITC
666 data are shown.

667

668 **Figure 5. Surface electrostatic potential of BmGH31 and EfGH31.**

669 (A) The homology model of BmGH31 was generated using the SWISS-MODEL server with
670 the EfGH31 coordinate complexed with GalNAc (PDB 6M77). The ribbon models of the N-
671 domain (10–230), A-domain (231–566), A'-subdomain (263–302), proximal C-domain (567–
672 657), distal C-domain (656–832), and FN3 domain (833–916) are shown in *blue, red, cyan,*
673 *orange, and pink,* respectively. (B and C) The surface electrostatic potential of BmGH31 (B)
674 and EfGH31 (C).

675

676 **Figure 6. Homology model showing the active site of BmNag31 and binding site of**
677 **CBM32s.**

678 Homology model of the active sites of BmNag31, BmCBM32, and EfCBM32 were generated
679 using the SWISS-MODEL server. (A) The BmGH31 homology model (*magenta*) is
680 superimposed on the EfGH31 complexed with GalNAc (PDB 6M77) (*cyan*). Side chains of
681 amino acid residues interacting with GalNAc are shown in stick model and GalNAc is shown
682 in yellow stick model. The conserved residues of BmGH31 are labeled and the residue (Leu492)
683 of EfGH32 corresponding to Val444 of BmGH31 is highlighted in *cyan*. N and A/B mean
684 nucleophilic and acid/base catalytic residues, respectively. (B) The homology models of
685 BmCBM32 (*magenta*) and EfCBM32 (*cyan*) are superimposed on the crystal structures of
686 CpCBM32-1 (PDB 4LPL, *red*) and CpCBM32-3 in complex with GalNAc (4P5Y, *orange*). The
687 residues predicted to bind GalNAc (*yellow*) are labeled with the same colors as the stick models.

688 **Supporting Information**

689

690 **Figure S1. Predicted subcellular localization of BmNag31.** Subcellular localization of
691 BmNag31 predicted by ngLOC (King et al., 2012) and visualized by SilkDB3.0 web server
692 (<https://silkdb.bioinfotoolkits.net>) is shown in (A). Hierarchical tree (B) and protein regions
693 important for the subcellular localization (C) were generated by DeepLoc-1.0 web server
694 (<http://www.cbs.dtu.dk/services/DeepLoc>).

695

696 **Figure S2. Multiple sequence alignment of Nag31 proteins from Lepidoptera and**
697 ***Enterococcus faecalis*.** Sequence alignment was performed using the ClustalW program, and
698 the figure was generated using ESPript 3.0. Catalytic residues and amino acid residues directly
699 interacting with GalNAc were predicted from the crystal structure of EfNag31A and are
700 highlighted by *blue stars* and *green triangles*, respectively. The signal peptide of EfNag31A is
701 indicated by the *black square*.

702

703 **Figure S3. SDS-PAGE analysis of the recombinant proteins expressed in *E. coli*.** (A) SDS-
704 PAGE of MBP-BmNag31. M, protein marker; lane 1, crude extract; lane 2, first affinity
705 chromatography with amylose resin; lane 3, second affinity chromatography with Ni-NTA
706 agarose. (B) SDS-PAGE of BmGH31. M, protein marker; lane 1, crude extract; lane 2,
707 BmGH31 purified with Ni-NTA agarose.

708

709 **Figure S4. Chromatogram of gel filtration.** Proteins are applied to a HiLoad 16/60 Superdex
710 200 prep grade column and eluted with 20 mM sodium phosphate buffer (pH 7.0) containing
711 300 mM NaCl. Colors and lines of chromatograms are follows: MBP-BmNag31, *blue line*;
712 BmGH31, *red line*; blue dextran 2000, *gray line*; molecular weight marker (thyroglobulin,
713 ferritin, aldolase, conalbumin, and ovalbumin), *gray dashed line*.

714

715 **Figure S5. Hydrolytic activity of BmGH31 toward bovine submaxillary mucin.** Bovine
716 submaxillary mucin (BSM) with or without pretreatment of neuraminidase, β -galactosidase,
717 and β -*N*-acetylhexosaminidase was incubated with BmGH31, and then analyzed by TLC.

718 Released *N*-acetylneuraminic acid (Neu5Ac) and GalNAc were indicated by arrows.

719

720 **Figure S6. Effects of temperature and pH on the hydrolysis of GalNAc α -pNP by MBP-**
721 **BmNag31 and BmGH31.** pH dependence (A), temperature dependence (B), pH stability (C),
722 and thermostability (D) of MBP-BmNag31 and BmGH31. pH dependence was measured in
723 McIlvaine buffer at pH 4.0–8.0 or in glycine-HCl buffer at pH 9.0–10.0. Temperature
724 dependence was examined in 50 mM sodium phosphate buffer (pH 6.5) at 20°C–60°C. pH
725 stability was measured at 30°C after incubating for 20 hours in McIlvaine buffer at pH 4.0–8.0
726 or in glycine-HCl buffer at pH 9.0–10.0 and 4°C. Thermostability was measured at 30°C after
727 incubation in 50 mM sodium phosphate buffer containing 300 mM NaCl (pH 6.5) at 4°C–60°C.
728 Symbols used are as follows: MBP-BmNag31, *filled circle*; BmGH31, *open circle*. All
729 experiments were performed in triplicate.

730

731 **Figure S7. Multiple sequence alignment of CBM32 proteins showing GalNAc binding**
732 **activity.** Sequence alignment was performed using the ClustalW program, and the figure was
733 generated using ESPript 3.0. Among amino acid residues involved in GalNAc recognition of
734 CpCBM32-1 (denoted by asterisks), amino acid residues that are also conserved among
735 BmCBM32, EfCBM32, and CpCBM32s are highlighted in yellow.

736

737 **Table S1. Primers used in this study.**

738

Ikegaya et al. Fig. 1

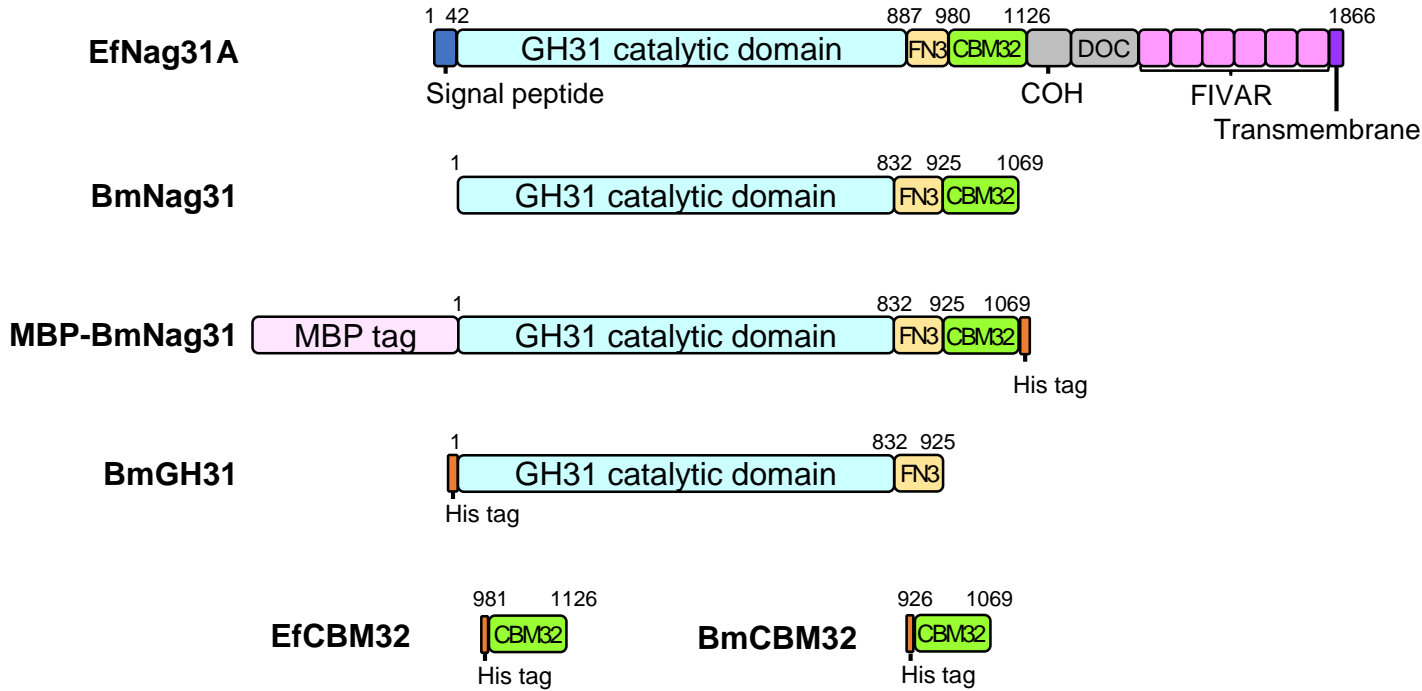


Figure 1. Modular architectures of native and recombinant proteins of BmNag31 and EfNag31A.

BmNag31 and EfNag31A refer to the native form of these enzymes, and the other names refer to the recombinant proteins that were expressed in *E. coli* and used in this study. Colors represent the following: signal peptide, *blue*; GH31 catalytic domain, *pale blue*; fibronectin type 3 (FN3) domain, *yellow*; carbohydrate-binding module 32 (CBM32) domain, *green*; Type III cohesin-like domain (COH) and dockerin-like domain (DOC), *gray*; FIVAR domain, *pink*; transmembrane, *purple*; His tag, *orange*; and maltose binding protein (MBP) tag, *light pink*.

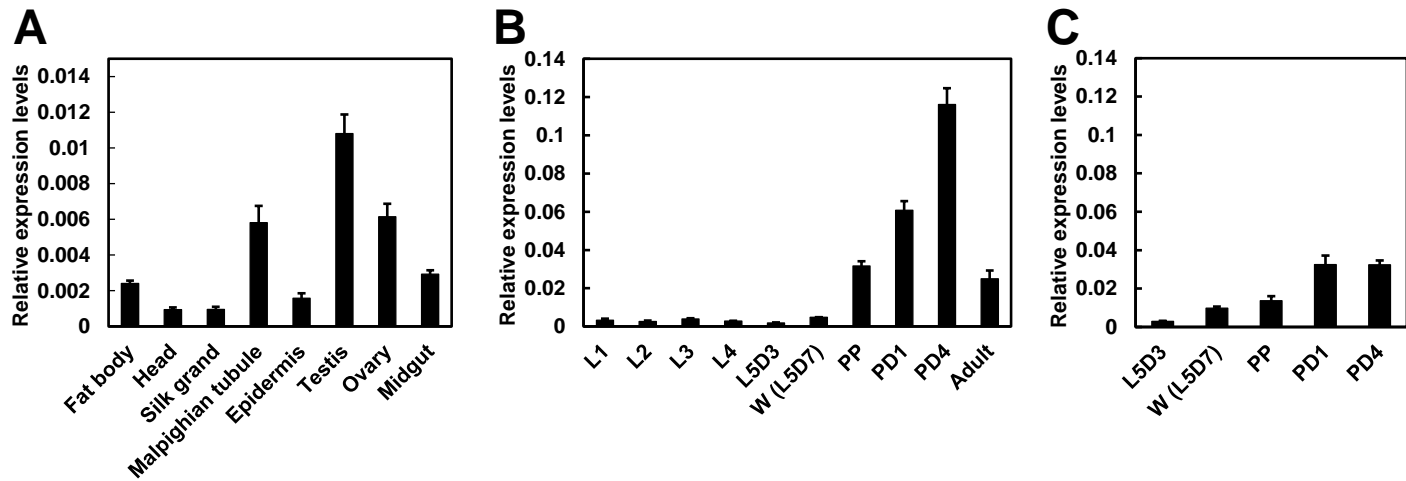


Figure 2. Expression *BmNag31* gene in different organs and developmental stages.

Relative expression levels of *BmNag31* in each organ in day-3 fifth-instar larvae (A), whole body of first instar larvae to adult stages (B), and midgut from day-3 fifth-instar larvae to day-4 pupae (C) were analyzed using quantitative RT-PCR. The housekeeping gene *BmGAPDH* was used as the internal control. Abbreviations: L1 to L5, first- to fifth-instar larval stages; PP, prepupal stage; P, pupal stage; D, day; W, wandering stage (day-7 fifth-instar larval stage). All experiments were performed in triplicate.

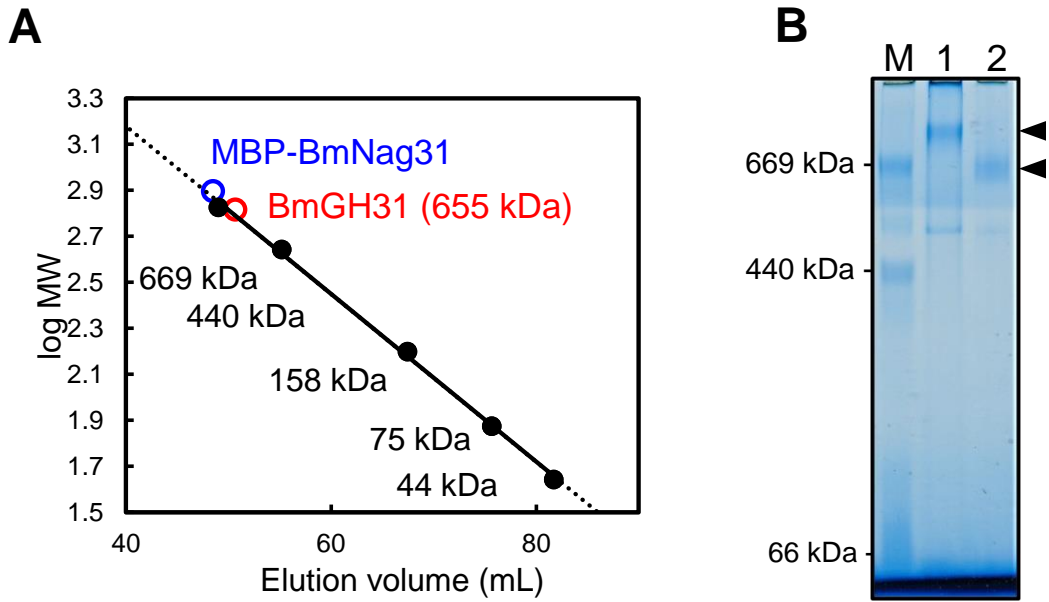


Figure 3. Oligomerization analysis of BmNag31.

The oligomeric state of BmNag31 was examined by gel filtration chromatography (A) and blue native PAGE (B). The experimental conditions are described in the Materials and Methods section. (A) Colors and lines of chromatograms are follows: MBP-BmNag31, *blue* line; BmGH31, *red* line; Blue dextran, *gray* line; molecular weight marker, *gray* dashed line. (B) A 3%–10 % gradient acrylamide gel was used for blue native PAGE. Lane M, marker; lane 1, MBP-BmNag31; lane 2, BmGH31. MBP-BmNag31 and BmGH31 were highlighted by arrows.

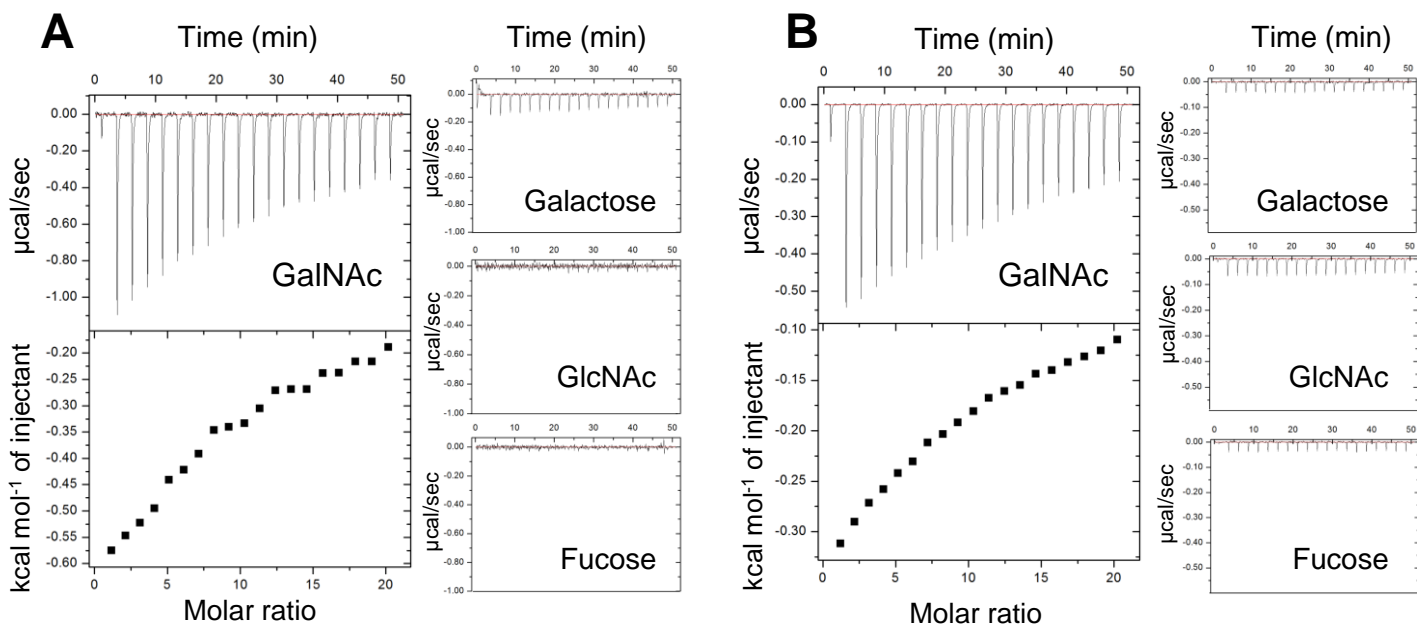


Figure 4. Binding activity of CBM32.

Binding activity of BmNag31 (A) and EfNag31A (B) toward GalNAc, D-galactose, GlcNAc, and L-fucose. The results of binding analysis of CBM32 and toward GalNAc show the raw ITC data (upper panels) and integrated heat of binding obtained from the raw data (lower panels). For the other results using D-galactose, GlcNAc, and L-fucose as ligands, only the raw ITC data are shown.

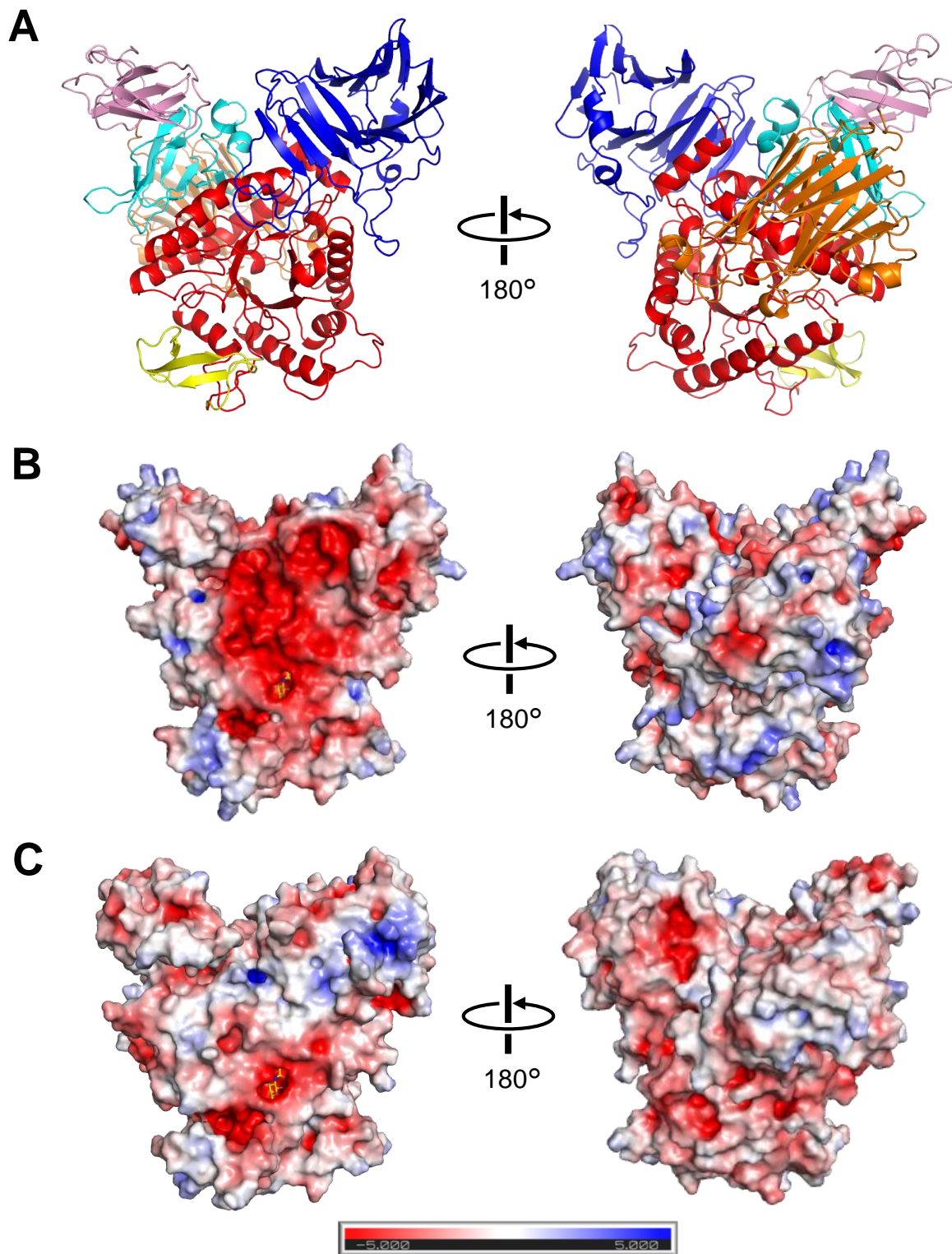


Figure 5. Surface electrostatic potential of BmGH31 and EfGH31.

(A) The homology model of BmGH31 was generated using the SWISS-MODEL server with the EfGH31 coordinate complexed with GalNAc (PDB 6M77). The ribbon models of the N-domain (10–230), A-domain (231–566), A'-subdomain (263–302), proximal C-domain (567–657), distal C-domain (656–832), and FN3 domain (833–916) are shown in *blue*, *red*, *cyan*, *orange*, and *pink*, respectively. (B and C) The surface electrostatic potential of BmGH31 (B) and EfGH31 (C).

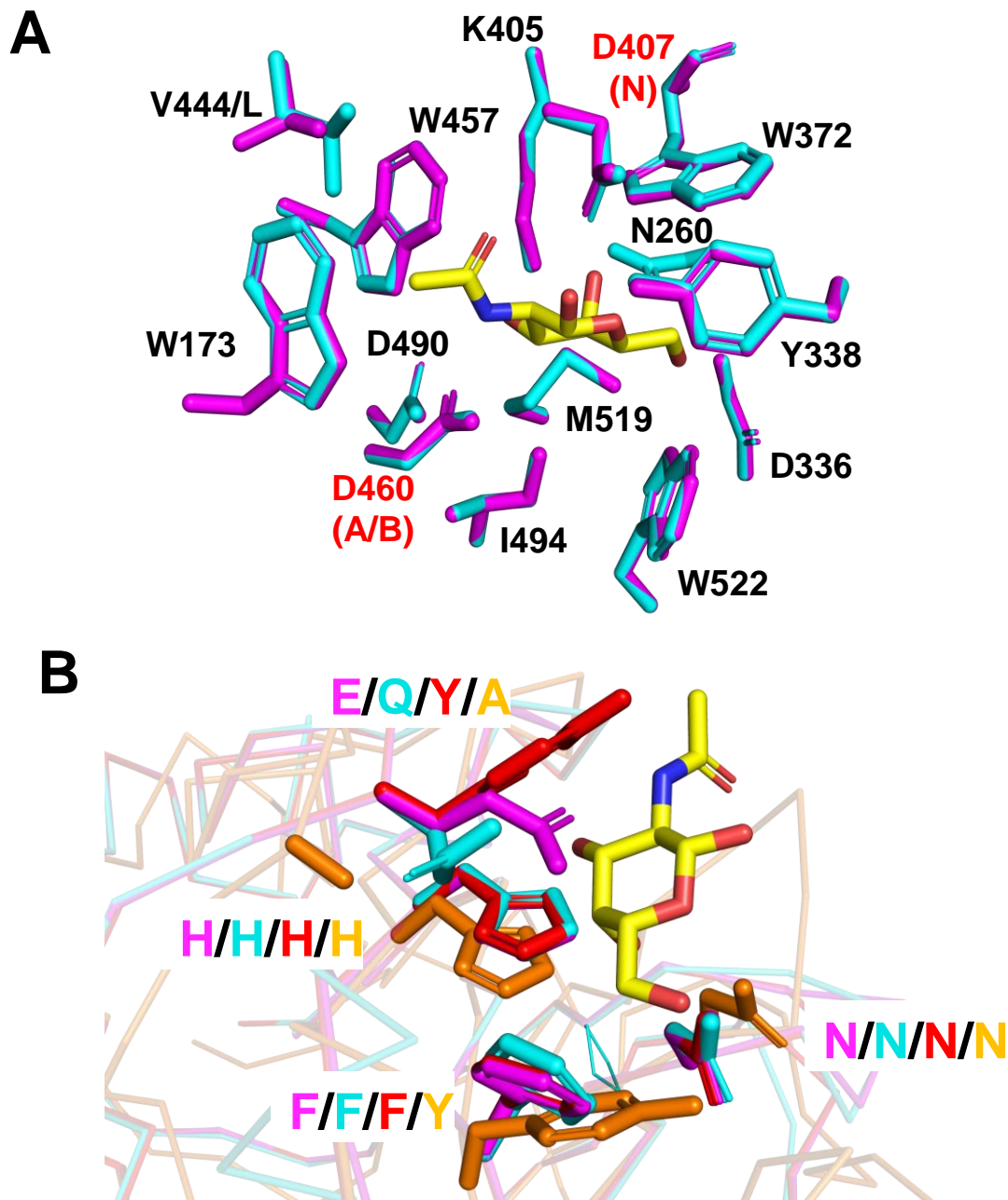


Figure 6. Homology model showing the active site of BmNag31 and binding site of CBM32s.

Homology model of the active sites of BmNag31, BmCBM32, and EfCBM32 were generated using the SWISS-MODEL server. (A) The BmGH31 homology model (*magenta*) is superimposed on the EfGH31 complexed with GalNAc (PDB 6M77) (*cyan*). Side chains of amino acid residues interacting with GalNAc are shown in stick model and GalNAc is shown in yellow stick model. The conserved residues of BmGH31 are labeled and the residue (Leu492) of EfGH32 corresponding to Val444 of BmGH31 is highlighted in *cyan*. N and A/B mean nucleophilic and acid/base catalytic residues, respectively. (B) The homology models of BmCBM32 (*magenta*) and EfCBM32 (*cyan*) are superimposed on the crystal structures of CpCBM32-1 (PDB 4LPL, *red*) and CpCBM32-3 in complex with GalNAc (4P5Y, *orange*). The residues predicted to bind GalNAc (*yellow*) are labeled with the same colors as the stick models.